COBEM 2021 26th International Congress of Mechanical Engineering
November 22-26, 2021, Virtual Congress, Brazil

COB-2021-0067
ROTOR VIBRATION CONTROL USING HYDRODYNAMIC BEARING WITH ACTIVE PADS

Heitor Antônio Pereira da Silva
Rodrigo Nicoletti
University of São Paulo, School of Engineering of São Carlos, Trabalhador São Carlense 400, 13566-590, São Carlos, SP, Brazil
heitorantonio@usp.br, rnicolet@sc.usp.br

Abstract. *Large rotating machines are elements of great importance to the production chain and they can eventually operate under unpredicted or off-the-norm conditions, thus resulting in failure and in significant economic losses. One way of reducing the consequences of such off-the-norm operation of these machines is the modification of the characteristics of the bearings that support the rotor. However, with conventional bearings, this is only possible through complete stops of the machine, which also result to economic losses. The solution to this problem comes from the development of active bearings that can change the dynamic characteristics of the machine during operation without needing machine stops. In this sense, the present work presents a tilting-pad journal bearing whose pads are controlled by electromagnetic actuators (an innovative design solution). By mounting the electromagnetic actuators in the bearing casing, behind the pads, one can exert electromagnetic forces on the pads and make them change their angular position in relation to the bearing. Hence, one can modify the dynamic characteristics of the rotor-bearing system for desired and more appropriated values for a given operational condition, thus reducing the need of machine stops and the consequent economic losses. In this work, we present the mathematical model of such system and numerical simulations of the system in open- and closed-loop conditions. The bearing and the rotor are modeled by rigid-body dynamics, and the lubricant interface is modeled by the Reynolds equation. The dynamics of the electromagnetic actuators are identified experimentally and used in the model as a transfer function representation. A proportional-derivative controller is adopted in the closed-loop simulations.*

Keywords: *active bearing, tilting-pad bearing, electromagnetic actuator, lateral vibration, rotor dynamics*

1. INTRODUCTION

The design of large rotating machines must obey demanding requirements and standards. Nevertheless, they can eventually operate under unpredicted or off-the-norm conditions. As a result, unscheduled downtime occurs to carry out the maintenance of the machine, resulting in large economic losses for the Industry. For example, dynamic instabilities in a compressor operated by Philips Petroleum Co. on an oil platform in the North Sea delayed production for six months (Ehrich and Childs, 1984); the costs of repairing seals, whose wear was caused by vibrations of the rotor, in a single Swissair aircraft turbine reached 1% of the company's annual cost of fuel (Bartha, 2000); the increase of the lateral vibration of the rotor of a 28 MW gas turbine in a thermoelectric power plant led to such a catastrophic failure which made its repair unfeasible (Farrahi *et al.*, 2011); gas turbines in a power plant operated by Petrobras in Bahia (Brazil) failed by excessive rotor vibration and it caused power generation suppression, thus harming the local population and leading to financial penalties for the company (Fontes and Budman, 2017); the excess of vibration of a propeller stage of a turbocharger operated by Petrobras caused the complete rupture of the stage, not allowing its repair (Azevedo *et al.*, 2016); high levels of vibration in a Petrobras hydrogen compressor made the machine stop, and consequently the production, when it was operating at full load (Brandão *et al.*, 2018).

As we can see in the power generation sector, medium and large rotating machines, such as turbogenerators, compressors, turbines and pumps, are essential for the production process. Therefore, these machines must have not only high performance, but also high security and availability (Perera *et al.*, 2019). In this case, the improvement of tilting-pad hydrodynamic bearings can represent the way to obtain more efficient machines. For example, a natural gas compressor on a platform in the Campos Basin (Brazil) presented high levels of sub-synchronous vibration when operating at full load. The solution to the problem came through changes in the tilting-pad hydrodynamic bearings (Li *et al.*, 2002).

The problem with this type of solution (the change in the characteristics of the tilting-pad hydrodynamic bearing) is necessity to completely stop the machine to exchange the bearing components, which inevitably results in financial losses. This is because these bearings are designed to present specific dynamic characteristics, which cannot be changed after manufacturing. An alternative way to give more flexibility to the operating conditions of tilting-pad hydrodynamic bearings, and consequently to the operating conditions of the machine, is to introduce actuator elements in the bearing, thus making them *active bearings*.

The first ideas of actively controlling vibrations in rotating systems emerged through the use of magnetic bearings. Magnetic bearings have the advantage of acting without contact, in a wide range of frequencies, and they are considered clean systems because there is no need to have any kind of lubricating fluid (other than air) at the interface between the rotor and the bearing (Maslen and Schweitzer, 2009). However, magnetic bearings become expensive when applied to large rotating systems. In these cases, the forces involved are high and the magnetic system becomes complex and bulky. In addition, protection systems must be implemented (auxiliary bearings) for the case of electrical failures or excessive loading on the bearing. Therefore, magnetic bearings (alone) are not the most recommended for application on large rotating machines.

In this context, a potential solution is proposed in which electromagnetic actuators are embedded in the pads of the bearings Viveros and Nicoletti (2014). In this case, the idea was to take advantage of the load capacity and stability of the tilting-pad hydrodynamic bearing to support the rotor, together with the actuation capacity of the actuators installed in the pads. By using the tilting-pad bearing as the support mechanism (hydrodynamic lubrication), the size of the magnetic actuator was reduced as it became a mechanism of sole vibration control (no rotor support). A safety system was no longer necessary.

The experimental results of this type of bearing showed an effective reduction in the vibration levels of the rotor, both in the domain of time (Moraes and Nicoletti, 2010) and in the domain of frequency (Viveros and Nicoletti, 2014). However, it was observed that the system presented a dynamic coupling between the electromagnetic forces and the angular movements of the pad. When actuators were turned on, the forces that attracted the rotor towards the pad, by reaction, attracted the pad towards the rotor, thus causing a torque on the pad and, consequently, changing its angular position. This dynamic coupling between the control forces and the positioning of the pads significantly changed the dynamics of the rotor-bearing system and jeopardized the effectiveness of rotor control.

An alternative way to improve the system is to modify the location of electromagnetic actuators inside the hydrodynamic bearing. The new position of electromagnetic actuators are in the bearing's housing, so that the electromagnetic force act on the external face of the pivoted pads (Fig. 1 – hydrodynamic bearings with active pads). Hence, the actuation and control forces no longer act on the rotor, but on the pads. The angular movement of the pad, caused by the electromagnetic actuator, will affect the hydrodynamic pressure distribution in the radial clearance between the pad and the rotor, thus causing an alteration in the balance of forces on the rotor. By Adopting an appropriately control strategy, this change in the balance of forces on the rotor can change the static and dynamic characteristics of the rotor-bearing system.

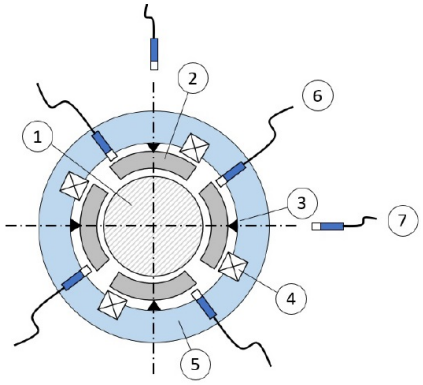

Figure 1. Hydrodynamic bearing with active pads: 1) rotor, 2) pad, 3) pivot, 4) electromagnetic actuators, 5) housing, 6) pad proximity sensor, 7) rotor proximity sensor.

In this work, we present the mathematical model of the hydrodynamic bearing with active pads. We model the system with two pads in the vertical direction (a simplification for concept proof purposes). The hydrodynamic forces are calculated by solving the Reynolds equation in each pad for a give operating condition. The system is numerically simulated subjected to unbalance perturbations. The effect of the active pads is analyzed by adopting a Proportional-Derivative (PD) control strategy. The results show the feasibility of the system in controlling and attenuating the rotor lateral vibrations.

2. MATHEMATICAL MODELING OF THE ACTIVE BEARING

The Hydrodynamic TPJB used in this work is composed for two tilting-pads in the vertical direction, as illustrated in Fig. 2a. The rotor is mounted in a pivoted lever, thus restraining the degrees of freedom of the rotor to vertical displacements. The lower and upper pads will be mounted on the bearing with their respective electromagnetic actuators. The structure that supports the rotor, and restricts its movements to vertical direction, will be used to impose both static and dynamic loads on the rotor, as shown in Fig. 2a.

The pressure distribution in the bearing gap over each pad is obtained by numerically solving the Reynolds equation

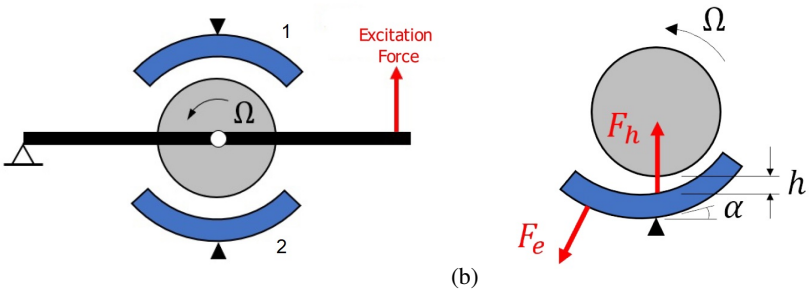

(a) (b)

Figure 2. Hydrodynamic bearing with two active pads: (a) pads in the vertical direction and rotor mounted in a pivoted lever, (b) electromagnetic force acting on the pad and hydrodynamic force acting on the rotor.

(Hamrock *et al.*, 2004):

$$\frac{\partial}{\partial y}\left(\frac{h_i^3}{\mu}\frac{\partial p_i}{\partial y}\right)+\frac{\partial}{\partial z}\left(\frac{h_i^3}{\mu}\frac{\partial p_i}{\partial z}\right)=6U\frac{\partial h_i}{\partial y}+12\frac{\partial h_i}{\partial t} \tag{1}$$

where $p_i(y,z)$ is the pressure of the oil film on the surface of the i-th pad, $h_i(y)$ is the thickness of the oil film between the rotor and the i-th pad, μ is the dynamic viscosity of the oil, U is the tangential velocity of the rotor's surface, t is time, and (y,z) is a local coordinate system on the surface of the pad.

The thickness of the oil film along the surface of the i-th pad can be obtained from the expression (Russo, 1998):

$$h_i(y)=R_s-R-[Y_r\cos\varphi_i+\alpha_i(R_s+h_s)]\,\text{sen}\left(\frac{y}{R_s}\right)-(Y_r\sin\varphi_i+R_s-R-h_o)\cos\left(\frac{y}{R_s}\right) \tag{2}$$

where R_s is the radius of the pad, R is the radius of the rotor, Y_r is the position of the rotor in the vertical direction, φ_i is the angular position of the pivot of the i-th pad, α_i is the angular position of the i-th pad, h_s is the pad thickness, and h_o is the nominal radial clearance.

The mathematical model of the electromagnetic actuators is the same as that presented in (Viveros and Nicoletti, 2014). Hence, the electromagnetic force is given by:

$$F_e=\left(\frac{\mathcal{I}}{d}\right)^2 \tag{3}$$

where $\mathcal{I}$ is the electric current in the electromagnetic actuator, and d is the distance between the actuator and the back surface of the pad. The electric current in the electromagnet is related to the electric voltage by the expression:

$$\mathcal{I}=\left(\frac{\mathrm{i}\omega\, a_1+a_0}{\mathrm{i}\omega\, b_1+b_0}\right)V(t) \tag{4}$$

where $V(t)$ is the electric voltage applied to the actuator, and (a_1,a_0,b_1,b_0) are the dynamic parameters of the electromagnetic actuator.

Hence, by giving an electric voltage, one calculates the resultant electric current $\mathcal{I}$ and the electromagnetic force F_e with Eqs.(3) and (4). This force, is applied to the back surface of the pads, thus causing a moment on the pad, as shown in Fig. 2b. This moment affects the angular position of the pad, thus altering the oil film thickness over the pad. The resultant hydrodynamic force on the pads is calculated by Eq.(1), and one obtains the resultant hydrodynamic force on the rotor (F_h – Fig. 2b). By applying a balance of forces on the system, using the Newton and Euler equations, one derives the equations of motion of the system as follows:

$$\begin{cases} I_L\ddot{\theta}=F_hL_r-m_rg+F_{ext}L_f \\ I_s\ddot{\alpha}_1=F_{e1}L_e-F_{ht1}h_s \\ I_s\ddot{\alpha}_2=F_{e2}L_e-F_{ht2}h_s \end{cases} \tag{5}$$

where I_L is the moment of inertia of the lever in relation to its pivot, θ is the angular displacement of the lever, F_h is the resultant hydrodynamic force acting on the rotor, L_r is the distance of the rotor to the pivot of the lever, m_r is the mass of the rotor, g is the acceleration of gravity, F_{ext} is the excitation force applied to the lever, L_f is the distance of the excitation force to the pivot of the lever, I_s is the moment of inertia of the pad, F_{ei} is the electromagnetic force applied to the i-th pad, L_e is the distance between the electromagnetic force and the pivot of the pad, and F_{hti} is the hydrodynamic force acting on the i-th pad in tangential direction.

3. NUMERICAL PROCEDURE

The mathematical model of the active bearing in study was implemented in MATLAB. The equations of motion of the system (Eq.(5)) are integrated in time using the command `ode15s`, which is a variable-step, variable-order (VSVO) solver based on the numerical differentiation formulas (NDFs) of orders 1 to 5, suitable for stiff problems (Shampine and Reichelt, 1997).

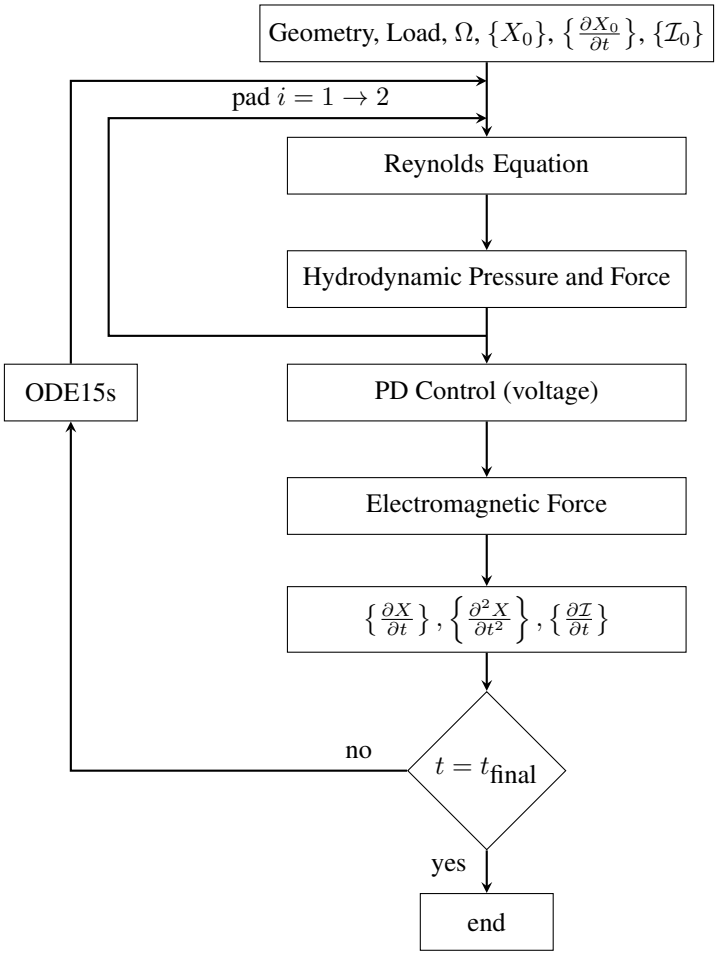

Figure 3. Flow chart of the algorithm used to simulate numerically the hydrodynamic bearing with active pads.

Figure 3 presents a flow chart of the algorithm, which can be described by the following steps:

1. input data: bearing geometry, bearing/rotor loading, rotating speed (Ω), initial positions of the rotor and pads $\{X_0\}$, initial velocity of rotor and pads $\left\{\frac{\partial X_0}{\partial t}\right\}$, initial current in the electromagnets $\{\mathcal{I}_0\}$;
2. calculate the thickness of the oil film on the i-th pad. The Finite Difference Method is applied to the Reynolds equation for the i-th pad, where ambient pressure is assumed at the boundary conditions and the Gümbel assumption is used as a cavitation model;
3. calculate the pressure distribution, and consequently the hydrodynamic forces. Steps 2 to 3 are repeated for the other pad;
4. obtain the control voltage to be applied to the actuators by adopting a Proportional-Derivative (PD) control strategy. For that, the position and velocity errors are determined from reference (desired) values;
5. determine the distance between each electromagnetic actuator and the respective pad. Calculate the resultant electromagnetic force acting on each pad;
6. use the equations of motion in Eq.(5) to calculate the higher order derivatives of the model;
7. if the current integration time is not equal to the final time t_{final}, the `ode15s` command continues the integration process, going back to step 2 in an iterative way. The higher order derivatives are used by the `ode15s` command to calculate the position $\{X\}$ of the system at a given time step t.

4. NUMERICAL RESULTS

The mathematical model is numerically integrated in time using the algorithm depicted in Fig. 3 and considering the parameter values listed in Table 1. These values refer to a rotor-bearing test rig at the Laboratory of Dynamics (EESC-USP).

The adopted control strategy is the PD control:

$$V(t) = -G_D\,\dot{e} - G_P\,e \tag{6}$$

where G_D and G_P are the derivative and proportional gains, respectively, and e is the error between the position of the rotor and the reference position of the rotor ($e = Y_r - Y_r^{\text{ref}}$).

In the present analysis, we adopted the values of 10^6 V.m^{-1} and 10^3 V.s.m^{-1} for the proportional and the derivative gains, respectively. These values were defined by trial-and-error to maximize the control effect (vibration attenuation) without exceeding the ± 10 V limits of the output ports in the acquisition system. Three excitation conditions are studied: external non-synchronous excitation, synchronous excitation (unbalance), oscillating control reference.

Table 1. Parameters of system used in the numerical simulations.

parameter	*value*	*unit*	*parameter*	*value*	*unit*
radial clearance (h_o)	100	μm	lever moment of inertia (I_L)	1.3	kg.m^2
rotor radius (R)	40	mm	rotor mass (m_r)	13.3	kg
pad inner radius (R_s)	40.2	mm	distance to rotor (L_r)	270	mm
pad thickness(h_s)	7	mm	distance to excitation (L_f)	540	mm
pad aperture angle	80	degree	distance to electromagnets (L_e)	60	mm
pad width	60	mm	parameter a_1	$a_1 = a_1(V)^*$	
pad moment of inertia (I_s)	0.00016	kg.m^2	parameter a_0	$a_0 = a_0(V)^*$	
pad pivot position (φ)	90 / 270	degree	parameter b_1	0.082	H
oil viscosity (μ)	0.032	N.s.m^{-2}	parameter b_0	2.6	Ω
preload factor	0.5	—			

* polynomial of the electric voltage (see details in Viveros and Nicoletti (2014)).

4.1 External Non-Synchronous Excitation

In this first analysis, we apply an excitation force at the lever, as shown in Fig. 2a. The applied force is non-synchronous, given by:

$$F_{ext} = 50\sin(2\pi f_{exc}\,t) \quad \text{N} \tag{7}$$

where f_{exc} is the frequency of excitation. We adopted the excitation frequencies of 10 and 50 Hz in the analysis, and we simulated the system for two rotating speeds: 600 and 2400 rpm. These rotating speeds represent a low speed and a high-speed operating condition of the system in study, respectively. The excitation frequencies of 10 and 50 Hz represent synchronous and super-synchronous excitations in the case of 600 rpm, respectively, whereas in the case of 2400 rpm they represent sub-synchronous and super-synchronous excitations. During the first 1 s of simulation, the control is turned off, after which the control is turned on. The reference for the controller (Y_r^{ref}) is the equilibrium position of the rotor at the operating rotating speed.

Figure 4 presents the positioning error of the rotor for the rotating speed of 600 rpm. As we can see in Fig. 4a (excitation frequency of 10 Hz), the rotor oscillates around the equilibrium position due to the excitation. When the control system is turned on at 1 s, we observe a significant reduction of the vibration amplitude (approximately 90% reduction). When the same system is excited by the same force at the frequency of 50 Hz (Fig. 4b), first we observe that the rotor response without control presents a smaller vibration amplitude than the previous case. That is a result of the higher damping of the hydrodynamic bearing at higher excitation frequencies. When the control system is turned on at 1 s, the vibration amplitude is reduced by approximately 50%. This worse performance of the control system at higher frequencies is a characteristics of the electromagnetic actuators, as previously observed in literature (Moraes and Nicoletti, 2010). Nevertheless, the control system managed to reduce the rotor vibration in both cases. The angular position of the pads in the bearing is presented in Fig. 5. When the control is turned on after 1 s, we observe in both cases of excitation that the electromagnetic forces move the pads towards higher angles.

Figure 6 presents the positioning error of the rotor for the rotating speed of 2400 rpm. As we can see in Fig. 6a (excitation frequency of 10 Hz), the rotor oscillates around the equilibrium position with a smaller amplitude than that of the rotating speed of 600 rpm (Fig. 4a). That is a consequence of the higher stiffness of the oil film at higher rotating

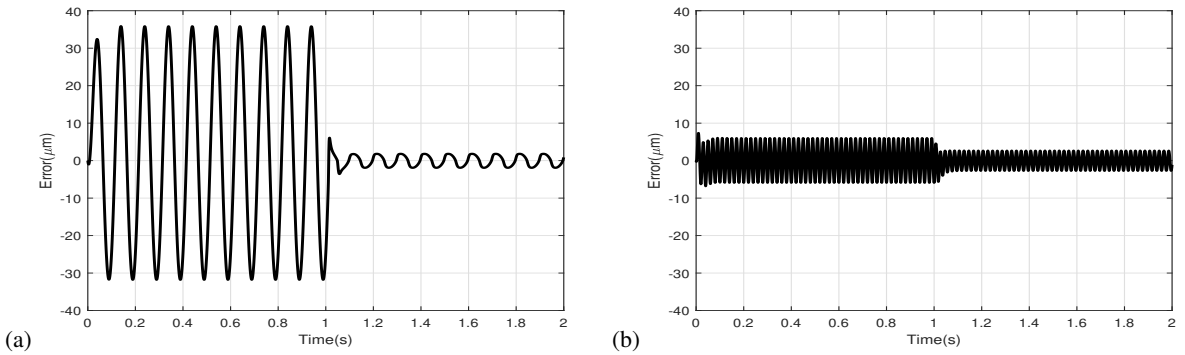

Figure 4. Positioning error of the rotor for the rotating speed of 600 rpm: (a) excitation frequency of 10 Hz, (b) excitation frequency of 50 Hz.

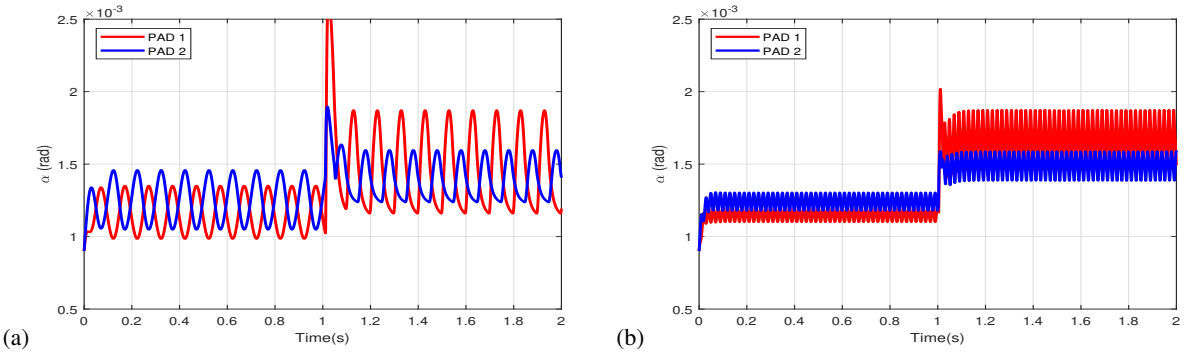

Figure 5. Angle of the pads in the active bearing at 600 rpm: (a) excitation frequency of 10 Hz, (b) excitation frequency of 50 Hz.

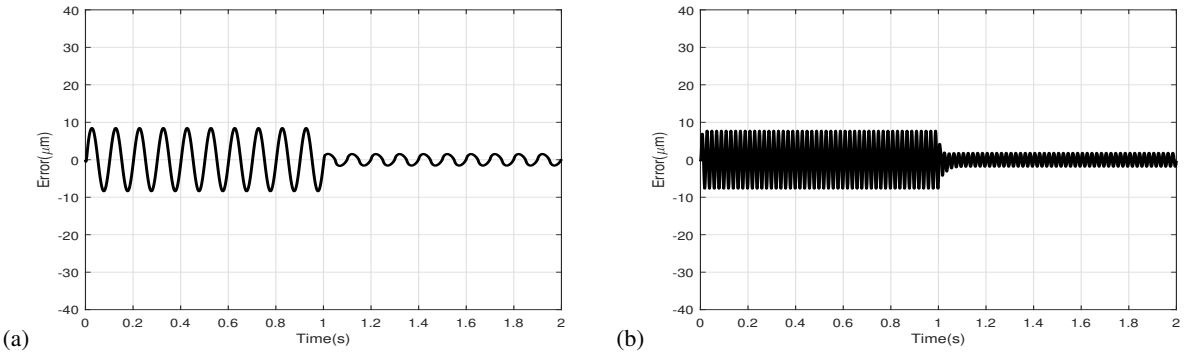

Figure 6. Positioning error of the rotor for the rotating speed of 2400 rpm: (a) excitation frequency of 10 Hz, (b) excitation frequency of 50 Hz.

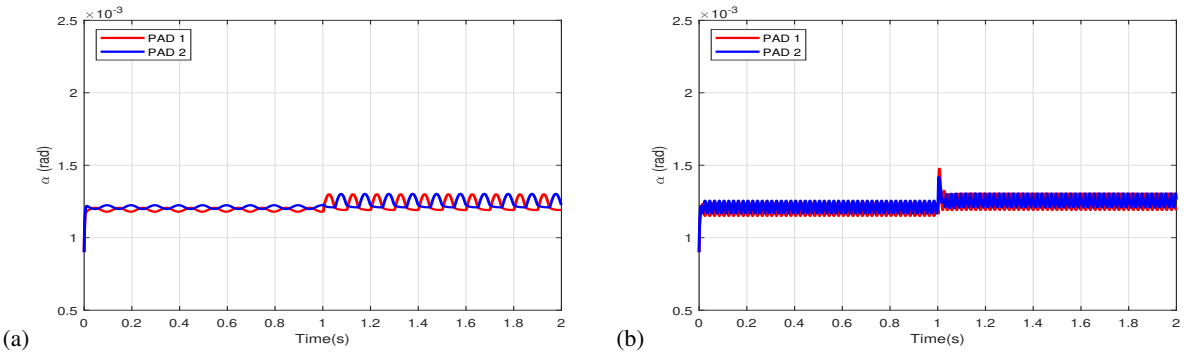

Figure 7. Angle of the pads in the active bearing at 2400 rpm: (a) excitation frequency of 10 Hz, (b) excitation frequency of 50 Hz.

speeds, thus leading the system to smaller responses under the same excitation. When the control system is turned on at 1 s, we observe a reduction of the vibration amplitude by approximately 70%. Although the percentage reduction is smaller than that of Fig. 4a, we observe that the controlled vibration amplitude is the same in both cases, around 5 μm peak-to-peak.

When the same system is excited by the same force at the frequency of 50 Hz (Fig. 6b), we observe that the higher damping of the hydrodynamic bearing at higher excitation frequencies reduces the vibration response of the rotor without control in comparison to the previous case. When the control system is turned on at 1 s, the vibration amplitude is reduced by approximately 60%. Again, the control system managed to reduce the rotor vibration in both cases. The angular position of the pads in the bearing is presented in Fig. 7. When the control is turned on after 1 s, we also observe in both cases of excitation that the electromagnetic forces move the pads towards higher angles, an evidence that the active pads are working to control the motion of the rotor.

4.2 Unbalance Excitation

The second analysis is an unbalance analysis. Hence, we consider that the excitation force is synchronous, applied at the position of the rotor, given by:

$$F_{unb} = m\varepsilon\Omega^2 \sin(\Omega t) \tag{8}$$

where $m\varepsilon$ is the unbalance value (0.004 kg.m), and Ω is the rotating speed (in rad/s). We adopted the rotating speeds of 600 and 3000 rpm. Again, the control is turned off during the first 1 s of simulation, after which the control is turned on. The reference for the controller (Y_r^{ref}) is also the equilibrium position of the rotor at the operating rotating speed. We also adopted the same values for the proportional and derivative gains.

Figure 8 presents the positioning error of the rotor for the two rotating speeds in study. For the rotating speed of 600 rpm (Fig. 8a), we observe a vibration reduction of approximately 70% when the control system is turned on. For the rotating speed of 3000 rpm (Fig. 8a), first we observe that the vibration response without control is much higher than that of the rotating speed of 600 rpm (a clear result of the higher unbalance forces at the rotating speed of 3000 rpm). When the control system is turned on, the vibration response is significantly reduced by approximately 80%. As we can see, the control system managed to reduce the rotor vibration in both cases.

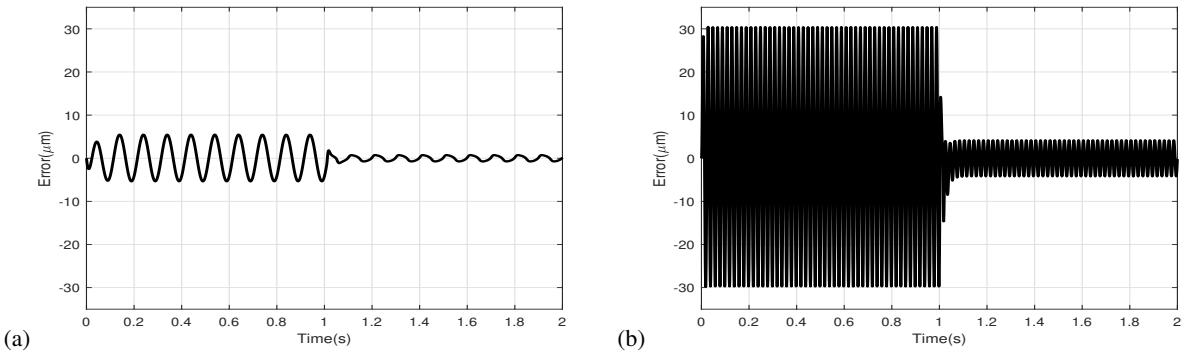

Figure 8. Positioning error of the rotor (unbalance response): (a) rotating speed of 600 rpm, (b) rotating speed of 3000 rpm.

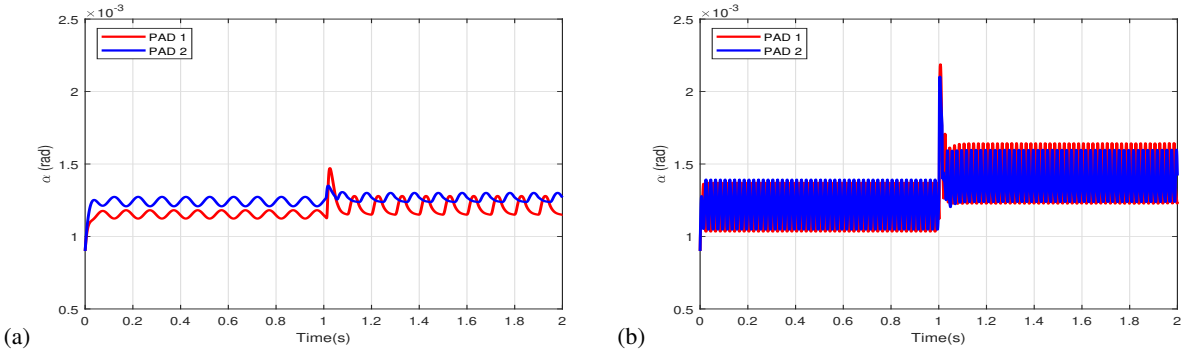

Figure 9. Angle of the pads in the active bearing (unbalance response): (a) rotating speed of 600 rpm, (b) rotating speed of 3000 rpm.

The angular position of the pads in the bearing for these cases is presented in Fig. 9. When the control is turned on

after 1 s, we also observe in both cases of unbalance excitation that the electromagnetic forces move the pads towards higher angles, i.e. the active pads are working to control the motion of the rotor.

4.3 Oscillating Position Reference

The third analysis involves the variation of the positioning reference in the controller. In this case, during the first 1 s of the simulation, the positioning reference for the controller is the equilibrium position of the rotor at the rotating speed. After 1 s, the positioning reference of the rotor is:

$$Y_r^{\text{ref}} = 10\sin(2\pi f_{exc}\, t) \quad \mu\text{m} \tag{9}$$

The adopted rotating speed is 600 rpm and two frequencies f_{exc} are adopted: 10 and 50 Hz. We adopt the same values for the proportional and derivative gains used in the previous analyses.

Figure 10 presents the positioning error of the rotor for both studied cases. During the first 1 s of simulation, the rotor remains at the equilibrium position and the error tends to zero. After 1 s, the reference starts oscillating according to Eq.(9). As one can see in Fig. 10, the control system follows the reference. However, the maximum amplitude of the reference is never achieved, and the performance of the controller worsens at higher frequencies (Fig. 10b). Again, this is an effect of the electromagnetic actuators, that lose performance as the frequency increases.

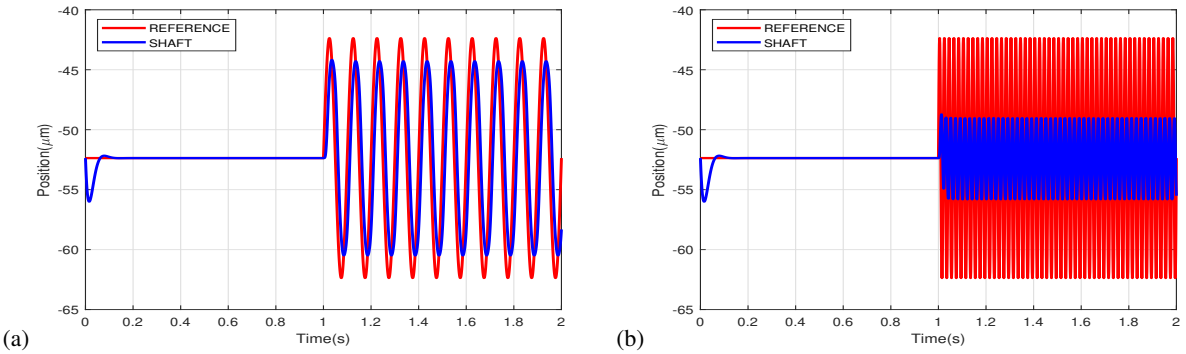

Figure 10. Rotor position at the rotating speed of 600 rpm: (a) reference at a frequency of 10 Hz, (b) reference at a frequency of 50 Hz.

5. CONCLUSION

In this work, we present the mathematical model of a tilting-pad journal bearing with active pads, i.e. with pads controlled by electromagnetic actuators. The numerical simulations presented in this work show the feasibility of the proposed active bearing in attenuating the vibration response of the rotor. By controlling the angular position of the pads with electromagnetic actuators, it was possible to reduce the vibration response of the rotor both under synchronous and non-synchronous excitation forces. In some cases, the reduction of vibration amplitude was significant (above 70%). Although very simple, the PD controller showed to be effective for attenuating the vibration of the rotor.

The electromagnetic actuators tend to lose performance (reduce actuation force) as the frequency increases. This effect had been observed in literature, and it was corroborated by the numerical results. When the excitation had higher frequency, the attenuation obtained with the active system was smaller than that under the same excitation at lower frequencies.

6. ACKNOWLEDGEMENTS

The authors acknowledge the support given to this project by FAPESP (Fundação de Amparo à Pesquisa do Estado de São Paulo), grant no. 2019/23220-2, CAPES (Coordenação de Aperfeiçoamento de Pessoal de Nível Superior), grant no. 88887.465094/2019-00, and CNPq (Coordenação Nacional de Desenvolvimento Científico e Tecnológico), under grant no. 301118/2018-3

7. REFERENCES

Azevedo, T.F., Cardoso, R.C., da Silva, P.R.T., Silva, A.S. and Griza, S., 2016. "Analysis of turbo impeller rotor failure". *Engineering Failure Analysis*, Vol. 63, pp. 12–20.

Bartha, A.R., 2000. *Dry friction backward whirl of rotors*. Ph.D. thesis, ETH Zurich.

Brandão, A., Rangel, J. and Melo, R., 2018. "Root cause investigation of high frequency structural vibration on a high pressure hydrogen compressor". In *International Conference on Rotor Dynamics*. Springer, pp. 366–379.

Ehrich, F. and Childs, D., 1984. "Self-excited vibration in high-performance turbomachinery".

Farrahi, G.H., Tirehdast, M., Abad, E.M.K., Parsa, S. and Motakefpoor, M., 2011. "Failure analysis of a gas turbine compressor". *Engineering Failure Analysis*, Vol. 18, No. 1, pp. 474–484.

Fontes, C.H. and Budman, H., 2017. "A hybrid clustering approach for multivariate time series–a case study applied to failure analysis in a gas turbine". *ISA transactions*, Vol. 71, pp. 513–529.

Hamrock, B.J., Schmid, S.R. and Jacobson, B.O., 2004. *Fundamentals of fluid film lubrication*. McGraw-Hill Co., New York.

Li, J., De Choudhury, P. and Tacques, R., 2002. "Seal and bearing upgrade for eliminating rotor instability vibration in a high pressure natural gas compressor". In *Turbo Expo: Power for Land, Sea, and Air*. Vol. 36096, pp. 1139–1151.

Maslen, E.H. and Schweitzer, G., 2009. *Magnetic bearings: theory, design, and application to rotating machinery*. Springer.

Moraes, D.C. and Nicoletti, R., 2010. "Hydrodynamic bearing with electromagnetic actuators: Rotor vibration control and limitations". In *Proceedings of ISMA 2010—International Conference on Noise and Vibration Engineering, Leuven, Belgium, September*. pp. 20–22.

Perera, L.P., Machado, M.M., Valland, A. and Manguinho, D.A., 2019. "Failure intensity of offshore power plants under varying maintenance policies". *Engineering Failure Analysis*, Vol. 97, pp. 434–453.

Russo, F.H., 1998. *Identificação das propriedades dinâmicas de mancais segmentados híbridos: teoria e experimento*. Master's thesis.

Shampine, L.F. and Reichelt, M.W., 1997. "The matlab ode suite". *SIAM Journal on Scientific Computing*, Vol. 18, pp. 1–22.

Viveros, H.P. and Nicoletti, R., 2014. "Lateral vibration attenuation of shafts supported by tilting-pad journal bearing with embedded electromagnetic actuators". *Journal of engineering for gas turbines and power*, Vol. 136, No. 4.

8. RESPONSIBILITY NOTICE

The authors are solely responsible for the printed material included in this paper.